Electrostatic-Force-Directed Assembly of Ag Nanocrystals onto Vertically Aligned Carbon Nanotubes†

Ganhua Lu, Liying Zhu, Pengxiang Wang, and Junhong Chen*

Department of Mechanical Engineering, University of Wisconsin−Milwaukee, 3200 North Cramer Street, Milwaukee, Wisconsin 53211

Dmitriy A. Dikin and Rodney S. Ruoff

Department of Mechanical Engineering, Northwestern University, 2145 Sheridan Road, Evanston, Illinois 60208

Ying Yu‡ and Z. F. Ren

Department of Physics, Boston College, 140 Commonwealth Avenue, Chestnut Hill, Massachusetts 02467

Received: February 23, 2007; In Final Form: June 15, 2007

A facile dry route electrostatic-force-directed assembly (ESFDA) was used to deposit silver nanocrystals onto the external surface of vertically aligned multiwalled carbon nanotubes (MWCNTs). Charged and nonagglomerated aerosol silver nanocrystals were first produced using a mini-arc plasma source. The nanocrystals were then assembled onto the electrically biased MWCNT array through the enhanced electric field near the CNT surface. The electrostatic field plays a crucial role in the assembly process. Gradients of the nanocrystal size and the nanocrystal areal density along the length of the CNT have been observed, and these are likely due to the variation of the electric field near the CNT surface. The ESFDA technique enables the in situ coating of CNT arrays with nanocrystals to create novel hybrid nanomaterials with tailored properties.

Introduction

Carbon nanotubes (CNTs)[1,2] have attracted interest because of their small diameter, large surface-to-volume ratio, great structural integrity, high electrical and thermal conductivity, good thermal and chemical stability, and exceptional strength and resilience.[3−5] Functionalization of CNTs with various chemical groups[6,7] and nanocrystals[8−11] can further enhance the properties of CNTs, and CNTs have been considered as superior supports for nanocrystal catalysts.[12,13] In fact, hybrid materials consisting of nanocrystals distributed on the surfaces of CNTs could potentially display not only the unique properties of nanocrystals[14,15] and those of nanotubes[16−18] but also additional novel properties. Recently, such CNTs with nanocrystals have been shown to be promising for various energy applications including solar cells,[19,20] fuel cells,[21,22] Li−ion batteries,[23] and hydrogen storage.[12,24]

Various methods have been developed to assemble nanocrystals onto CNTs. Most wet-chemistry strategies involve chemical functionalization of the CNT surface followed by the assembly of nanocrystals onto the CNTs via covalent,[25] noncovalent,[7] or electrostatic interactions.[9,26] Although the wet-chemistry methods work well with randomly dispersed CNTs, they are not suitable for vertically aligned CNTs; the aligned structure will be damaged in the wet processing because the upper ends of the neighboring nanotubes have been seen to bundle together and some nanotubes are caused to lie down.[27] Vertically aligned CNTs are of great interest for practical device applications because of potentially higher device efficiency and packing density. For instance, in fuel cells having metal catalyst nanocrystals coated on CNTs, the nature of the packing of loose CNT powders could substantially decrease the effective contact area between nanocrystals and reactants so as to decrease the metal catalytic activity. Substitution of loose CNT powders with aligned CNTs could overcome this disadvantage and increase the fuel-cell efficiency.

We have recently developed a material-independent dry route based on the electrostatic-force-directed assembly (ESFDA) to assemble aerosol nanocrystals onto CNTs.[28] In principle, the ESFDA technique works for both random CNTs and aligned CNTs without the need of chemical functionalization or other pretreatments of the CNTs. With this technique, we have demonstrated the successful assembly of various nanocrystals previously, including single-component nanocrystals (Au, Ag, and SnO_2)[28,29] and multicomponent nanocrystals (SnO_2 and Ag),[29] onto randomly dispersed MWCNTs and single-walled CNTs (SWCNTs). Charged and nonagglomerated aerosol nanocrystals were produced from a mini-arc plasma source[30] and then delivered to the electrically biased CNTs in an inert carrier gas. The electric field near the CNT surface was enhanced significantly, and the aerosol nanocrystals were attracted to the external surface of the CNTs. In addition to an intrinsic nanocrystal size selection during the assembly process, nanocrystal size and areal density on CNTs can be controlled by the bias on the CNTs and the flow residence time. In our earlier study, we noted that the CNTs have to be suspended in order to maximize the field enhancement that is critical to the assembly. Here we report the deposition of Ag nanocrystals onto vertically aligned MWCNTs using the ESFDA technique. The

† Part of the special issue "Richard E. Smalley Memorial Issue".

* Corresponding author. E-mail at jhchen@uwm.edu.

‡ Permanent Address: College of Physical Science and Technology, Huazhong Normal University, Wuhan, China 430079.

10.1021/jp071523x CCC: $37.00
Published on Web 08/14/2007

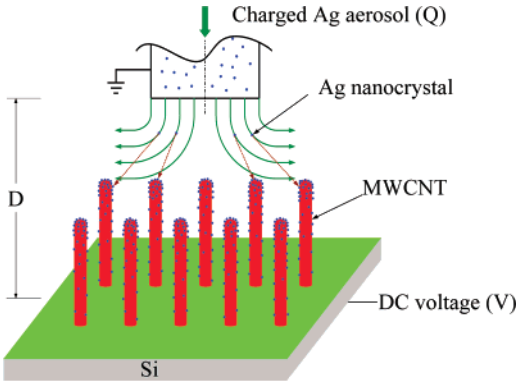

Figure 1. Schematic diagram for the assembly of Ag nanocrystals onto vertically aligned MWCNTs.

use of vertically aligned CNTs represents another means to realize the field enhancement. In fact, we have observed variations of nanocrystal size as well as nanocrystal areal density due to the variation of the electric field along the CNT length. The electric field near the CNTs is computed in an effort to develop an understanding of the experimentally observed distributions of nanocrystals on CNTs.

Experimental Method

Vertically aligned MWCNTs were grown on the silicon wafer with nickel catalysts by plasma-enhanced chemical vapor deposition (PECVD).[31,32] The Si wafer was first sputter-coated with a layer of Cr as a diffusion barrier layer, and then a layer of Ni catalyst was deposited onto Cr. The CNTs were about 10 μm in length and 150 nm in diameter. The average spacing between nanotubes was about 500 nm and thus the estimated areal density was 4×10^8 tubes/cm^2.

Aerosol Ag nanocrystals were generated through physical vaporization of solid precursor material (high-purity Ag wire purchased from ESPI) using a mini-arc plasma source sustained between a tungsten cathode and a graphite anode.[30] Most product Ag nanocrystals were nonagglomerated. A fraction of the as-prepared nanocrystals were electrically charged, possibly by the arc plasma or through thermionic emission of electrons from the crystal surface.[33] The nanocrystal size distribution was relatively broad, ranging from a few to tens of nanometers.

Figure 1 shows a schematic diagram of the assembly process. Silver nanocrystals were carried by an inert gas mixture (Ar/N_2) and delivered into an electrode gap to form a stagnation flow. The top electrode was a grounded metal tube that introduced the aerosol nanocrystals. The bottom electrode was a Si wafer with the vertically aligned MWCNTs that had been grown on it previously and was electrically biased with a constant voltage (-2 kV). The gap distance (D) between the two electrodes was about 2 mm. With the bias voltage applied to the aligned MWCNTs on the Si wafer, the electric field near the MWCNT surface was enhanced significantly, especially at the tips, and the oppositely charged Ag nanocrystals were attracted onto the surfaces of the MWCNTs.

Techniques including scanning electron microscopy (SEM), energy-dispersive X-ray spectroscopy (EDX), X-ray photoelectron spectroscopy (XPS), and transmission electron microscopy (TEM) were used to analyze the nanocrystal-coated MWCNT array. SEM studies were performed on a Nova NanoSEM 600 (FEI Co.). EDX was done on a TOPCON ABT-32 SEM with an EVEX low-element EDX analyzer. XPS was performed on a HP5950 ESCA spectrometer with monochromatic Al Kα radiation as the X-ray source. A Hitachi H 9000 NAR TEM

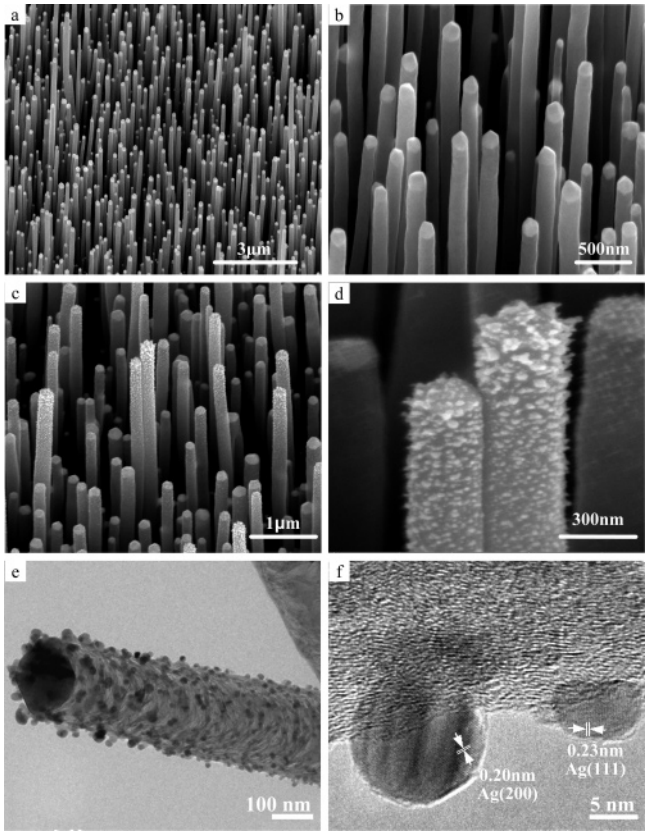

Figure 2. SEM images (a−d) of an as-grown MWCNT array on a silicon substrate at (a) lower magnification and (b) higher magnification; (c) evidence of nanocrystals coating MWCNTs at a lower magnification and (d) a higher magnification image of a region in image (c), showing nanocrystals deposited on the external surfaces and tips of the MWCNTs. (e) TEM image of a nanocrystal-coated MWCNT scratched from the Si wafer. (f) HRTEM image showing lattice fringes of Ag nanocrystals deposited on a MWCNT.

was used for analyses, with a point resolution of 0.18 nm at 300 kV in the phase-contrast high-resolution TEM (HRTEM) imaging mode. The TEM sample was prepared by scratching a small area of the product nanocrystal-coated MWCNTs off the Si wafer and then placing it onto a copper TEM grid.

Results and Discussion

The assembly of nanocrystals onto the CNT array is demonstrated by SEM and TEM images. As a comparison, Figure 2a,b shows the SEM images of as-grown, vertically aligned MWCNTs on a Si wafer. A catalyst particle containing Ni caps the tip of each CNT, preventing the assembly of nanocrystals onto the interior surface of the CNTs. The external surface of the CNTs appears smooth with no particles observed. Figure 2c shows a similar MWCNT array coated with Ag nanocrystals. The Ag nanocrystals are distributed on the outside surfaces of the CNTs and particularly on the upper portion of the aligned MWCNTs because of the strong field enhancement effect close to the tips. Evidence of these nanocrystals is seen in the higher-magnification SEM image shown in Figure 2d. Figure 2e shows a typical low-magnification TEM image of the nanocrystal-coated MWCNTs. Both the nanocrystal areal density and the average nanocrystal size maximize at the CNT tip, consistent with the SEM observation (Figure 2d). The CNT in Figure 2e bears a bamboo structure that is typical of the PECVD growth process.[34] The crystallinity of Ag nanocrystals on CNTs is confirmed by lattice fringes indexed in the HRTEM image of Figure 2f. The measured lattice spacings of 0.20 and

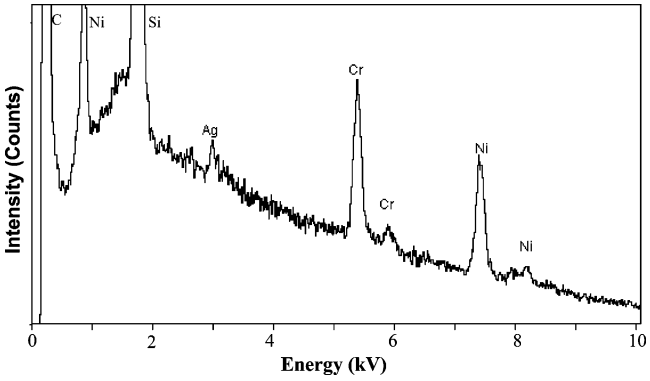

Figure 3. SEM-EDX spectrum of vertically aligned MWCNTs coated with Ag nanocrystals.

0.23 nm correspond to the (200) and (111) planes of silver crystal, respectively.

The hybrid Ag nanocrystal−CNT structures were examined with EDX and XPS. Figure 3 shows an EDX spectrum of the as-prepared sample with a tilted angle of 60° between the Si wafer and the electron beam. A weak silver signal is present in the spectrum in contrast to the stronger Cr, Ni, Si, and C peaks from the original aligned CNTs and the Si substrate because of the smaller amount of Ag in the sample. It is difficult to estimate the total amount of Ag accurately because of the changing Ag areal density caused by the uneven deposition from the varying electric field along the length of the CNT (discussed further below). Assuming a 10% surface coverage of Ag nanocrystals on the CNT surface, Ag represents only about 0.02% of the total sample mass. Figure 4 shows the XPS spectra of the aligned MWCNTs coated with Ag nanocrystals. The binding energies of 367.8 and 373.8 eV shown in Figure 4a correspond to the peaks of Ag $3d_{5/2}$ and $3d_{3/2}$ doublets,[35] respectively. Figure 4b shows the peak of C 1s core level with a binding energy of 284.6 eV.[35]

On the basis of our prior study,[28] the electric field and flow residence time are two critical parameters that govern the nanocrystal assembly process. In this study, the gas flow rate (total flow residence time) was fixed and it is thought that the electric-field distribution determines the final Ag nanocrystal distribution on the CNTs. There are varying CNT heights in the array shown in Figure 2. More crystals are distributed at the tips of taller CNTs likely because of a larger field enhancement for these taller CNTs, and perhaps also due to shadowing effects. The CNTs in the array are close to each other, and the proximity effect (field-screening effect) results in field enhancement only at the tip portion of the CNTs. A larger field enhancement is expected at the tips of taller CNTs. The higher electric field can attract larger nanocrystals with smaller electrical mobilities (for the same charge level on all nanocrystals).[28] The observed larger nanocrystals near the tip of CNTs suggest the critical role of the electric field on the assembly process because a shadowing effect, only, should not lead to the variation in nanoparticle size along the CNT length.

We have also observed a similar variation in nanoparticle areal density and size on isolated CNTs. Figure 5a shows a SEM image of an isolated CNT coated with Ag nanocrystals from the tip to the root. The upper portion of the tube is enlarged and shown in Figure 5b. Both the nanocrystal areal density and the average nanocrystal size decrease along the CNT from the tip to its root. For an isolated CNT, the proximity and shadowing effects are not present, and a variation of the nanocrystal distribution along the full tube length can only be attributed to

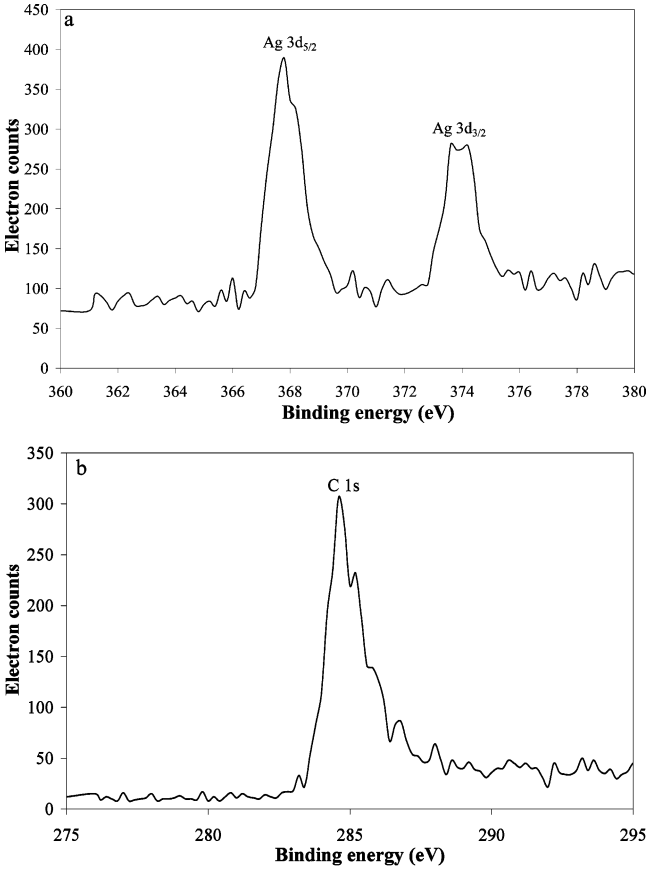

Figure 4. XPS spectra of (a) Ag 3d core levels and (b) C 1s core level of the aligned CNT array coated with Ag nanocrystals.

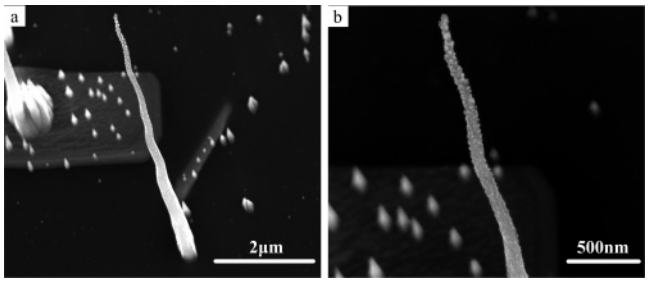

Figure 5. (a) SEM image of an isolated vertically aligned MWCNT coated with Ag nanocrystals, and (b) the enlarged view of the same MWCNT showing variations of the nanocrystal size and areal density along the length of the CNT.

the variation in the electric field along the tube axis. Therefore, our results clearly support the critical role of the electric field during the assembly process.

The electric-field distribution near the CNT surface was modeled in an attempt to potentially provide an understanding of the experimental observations. The vertical CNT was modeled as a cylinder with a hemispherical cap.[36,37] To simplify the model, a 2D computational domain with vertical CNT(s) against a flat plane is considered. The CNT is assumed to have the same dimensions as those used in the experiments, that is, 150 nm in diameter and 10 μm in length. The electric-field distribution over the domain is computed by numerically solving the Laplace equation using "charged particle optics software" (CPO version 5.2, CPO Ltd., 2004). The field enhancement factor (γ), which is defined as the ratio of the local field to that of the uniform field that would exist between two smooth plates

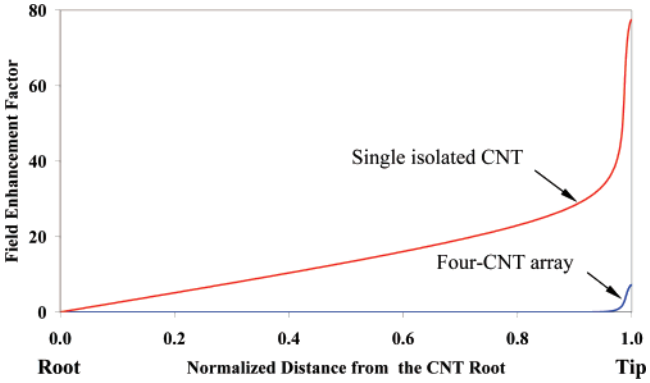

Figure 6. Electric-field-enhancement factor along the length of the CNT for a single isolated, vertically aligned CNT, and a four-tube square array with intertube spacing of 500 nm. The CNTs are 10 μm in length and 150 nm in diameter. The spacing between the CNT substrate and the counter electrode is 2 mm.

without the CNT(s) present, was obtained along the length of the CNT and is discussed further below.

The electric-field distribution was obtained for a single isolated CNT and for a four-tube square array having the same intertube spacing (500 nm) as that of the experimental sample. Figure 6 shows that γ monotonically increases from the root to the tip of the CNT in both cases. The field enhancement is much weaker for the four-tube array than for the isolated CNT because of the shielding effect, as expected. The modeling results are comparable to those published in the literature.[36,37] Such modeling points to the possible relevance of field enhancement as influencing the locations nanocrystals are deposited during the ESFDA process.

Conclusions

The ESFDA technique was used to assemble aerosol Ag nanocrystals onto the external surfaces of vertically aligned MWCNTs, as confirmed with SEM and TEM images and SEM-EDX and XPS spectra. The electric-field distribution near the CNT surface was computed using a simple model of the CNT as a cylinder with a hemispherical cap; the field-enhancement factor increases from the root to the tip of the CNT for the two cases studied. The areal density and size distributions of Ag nanocrystals observed along the CNTs in the vertical array can be rationalized by the variation of the electric field near the CNT surface; it is possible that shadowing effects also play a minor role on the variation in the nanocrystal areal density but not the nanocrystal size. Novel hybrid nanostructures prepared using the ESFDA technique may open up new opportunities for CNT applications.

Acknowledgment. We thank Marija Gajdardziska-Josifovska for providing TEM access, Donald Robertson for technical support with TEM analyses, and Steven Hardcastle for assistance with XPS analysis. J.C. is supported by the National Science Foundation through a SGER grant (Combustion, Fire, and Plasma Systems Program, Grant No. 0604079, Dr. Phillip R. Westmoreland, Program Director); R.S.R. and D.D. are supported by the National Science Foundation through an NER grant with J.C. (NER Program, Grant No. 0609059, Dr. Charalabos H. Doumanidis, Program Director); R.S.R., D.D., and Z.R. are supported by the National Science Foundation through a NIRT grant (NIRT Program, Grant No. 0304506, Dr. Ken P. Chong, Program Director); and Y.Y. is partly supported by China Scholarship Council and National Science Foundation of China (No. 90510012).

References and Notes

(1) Iijima, S. *Nature* **1991**, *354*, 56.
(2) Iijima, S.; Ichihashi, T. *Nature* **1993**, *363*, 603.
(3) Treacy, M. M. J.; Ebbesen, T. W.; Gibson, J. M. *Nature* **1996**, *381*, 678.
(4) Saito, R.; Dresselhaus, G.; Dresselhaus, M. S. *Physical Properties of Carbon Nanotubes*; Imperial College Press: London, 1998.
(5) Yu, M. F.; Lourie, O.; Dyer, M. J.; Moloni, K.; Kelly, T. F.; Ruoff, R. S. *Science* **2000**, *287*, 637.
(6) Agrawal, S.; Raghuveer, M. S.; Kroger, R.; Ramanath, G. *J. Appl. Phys.* **2006**, *100*, No. 094314.
(7) Li, L. Y.; Yang, Y.; Yang, G. L.; Chen, X. M.; Hsiao, B. S.; Chu, B.; Spanier, J. E.; Li, C. Y. *Nano Lett.* **2006**, *6*, 1007.
(8) Huang, Q.; Gao, L. *Nanotechnology* **2004**, *15*, 1855.
(9) Kim, B.; Sigmund, W. M. *Langmuir* **2004**, *20*, 8239.
(10) Lao, J. Y.; Li, W. Z.; Wen, J. G.; Ren, Z. F. *Appl. Phys. Lett.* **2002**, *80*, 500.
(11) Tang, H.; Chen, J. H.; Huang, Z. P.; Wang, D. Z.; Ren, Z. F.; Nie, L. H.; Kuang, Y. F.; Yao, S. Z. *Carbon* **2004**, *42*, 191.
(12) Anson, A.; Lafuente, E.; Urriolabeitia, E.; Navarro, R.; Benito, A. M.; Maser, W. K.; Martinez, M. T. *J. Phys. Chem. B* **2006**, *110*, 6643.
(13) Atwan, M. H.; Macdonald, C. L. B.; Northwood, D. O.; Gyenge, E. L. *J. Power Sources* **2006**, *158*, 36.
(14) Scher, E. C.; Manna, L.; Alivisatos, A. P. *Philos. Trans. R. Soc. London, Ser. A* **2003**, *361*, 241.
(15) Fissan, H.; Kennedy, M. K.; Krinke, T. J.; Kruis, F. E. *J. Nanopart. Res.* **2003**, *5*, 299.
(16) Dresselhaus, M. S.; Dai, H. J. *Mater Res. Soc. Bull.* **2004**, *29*, 237.
(17) de Heer, W. A. *Mater Res. Soc. Bull.* **2004**, *29*, 281.
(18) Dresselhaus, M. S.; Dresselhaus, G. and Avouris, P. *Carbon Nanotubes: Synthesis, Structure, Properties and Applications*; Springer-Verlag: Berlin, 2001.
(19) Landi, B. J.; Castro, S. L.; Ruf, H. J.; Evans, C. M.; Bailey, S. G.; Raffaelle, R. P. *Sol. Energy Mater Sol. Cells* **2005**, *87*, 733.
(20) Robel, I.; Bunker, B.; Kamat, P. V. *Adv. Mater* **2005**, *17*, 2458.
(21) Santhosh, P.; Gopalan, A.; Lee, K. P. *J. Catal.* **2006**, *238*, 177.
(22) Robel, I.; Girishkumar, G.; Bunker, B. A.; Kamat, P. V.; Vinodgopal, K. *Appl. Phys. Lett.* **2006**, *88*, 073113.
(23) Zhang, Y.; Zhang, X. G.; Zhang, H. L.; Zhao, Z. G.; Li, F.; Liu, C.; Cheng, H. M. *Electrochim. Acta.* **2006**, *51*, 4994.
(24) Yildirim, T.; Ciraci, S. *Phys. Rev. Lett.* **2005**, *94*, 175501.
(25) Zamudio, A.; Elias, A. L.; Rodriguez-Manzo, J. A.; Lope-Urias, F.; Rodriguez-Gattorno, G.; Lupo, F.; Ruhle, M.; Smith, D. J.; Terrones, H.; Diaz, D.; Terrones, M. *Small* **2006**, *2*, 346.
(26) Xing, Y. C. *J. Phys. Chem. B* **2004**, *108*, 19255.
(27) Ye, X. R.; Lin, Y. H.; Wai, C. M.; Talbot, J. B.; Jin, S. H. *J. Nanosci. Nanotechnol.* **2005**, *5*, 964.
(28) Chen, J. H.; Lu, G. H. *Nanotechnology* **2006**, *17*, 2891.
(29) Zhu, L. Y.; Lu, G. H.; Chen, J. H. *J. Heat Transfer* **2008**, *130*, in press.
(30) Chen, J. H.; Lu, G. H.; Zhu, L. Y.; Flagan, R. C. *J. Nanopart. Res.* **2007**, *9*, 203.
(31) Ren, Z. F.; Huang, Z. P.; Xu, J. W.; Wang, J. H.; Bush, P.; Siegal, M. P.; Provencio, P. N. *Science* **1998**, *282*, 1105.
(32) Huang, Z. P.; Wu, J. W.; Ren, Z. F.; Wang, J. H.; Siegal, M. P.; Provencio, P. N. *Appl. Phys. Lett.* **1998**, *73*, 3845.
(33) Wang, X.; Hafiz, J.; Mukherjee, R.; Renault, T.; Heberlein, J.; Girshick, S. L.; McMurry, P. H. *Plasma Chem. Plasma Process.* **2005**, *25*, 439.
(34) Wen, J. G.; Huang, Z. P.; Wang, D. Z.; Chen, J. H.; Yang, S. X.; Ren, Z. F.; Wang, J. H.; Calvet, L. E.; Chen, J.; Klemic, J. F.; Reed, M. A. *J. Mater Res.* **2001**, *16*, 3246.
(35) Wanger, C. D.; Riggs, W. M.; Davis, L. E.; Moulder, J. F.; Muilenberg, G. E. E. *Handbook of X-ray Photoelectron Spectroscopy*; Perkin-Elmer Corp.: Eden Prairie, MN, 1978.
(36) Podenok, S.; Sveningsson, M.; Hansen, K.; Campbell, E. E. B. *Nano* **2006**, *1*, 87.
(37) Read, F. H.; Bowring, N. J. *Microelectron. Eng.* **2004**, *73*−*74*, 679.